CrossMark

ORIGINAL PAPER

# Investigation on the Permeability Evolution of Gypsum Interlayer Under High Temperature and Triaxial Pressure

Meng Tao[1] · You Yechao[2] · Chen Jie[3] · Hu Yaoqing[1]

**Abstract** The permeability of the surrounding rock is a critical parameter for the designing and assessment of radioactive waste disposal repositories in the rock salt. Generally, in the locations that are chosen for radioactive waste storage, the bedded rock salt is a sedimentary rock that contains NaCl and $Na_2SO_4$. Most likely, there are also layers of gypsum ($CaSO_4 \cdot 2H_2O$) present in the salt deposit. Radioactive wastes emit a large amount of heat and hydrogen during the process of disposal, which may result in thermal damage of the surrounding rocks and cause a great change in their permeability and tightness. Therefore, it is necessary to investigate the permeability evolution of the gypsum interlayer under high temperature and high pressure in order to evaluate the tightness and security of the nuclear waste repositories in bedded rock salt. In this study, a self-designed rock triaxial testing system by which high temperature and pressure can be applied is used; the μCT225kVFCB micro-CT system is also employed to investigate the permeability and microstructure of gypsum specimens under a constant hydrostatic pressure of 25 MPa, an increasing temperature (ranging from 20 to 650 °C), and a variable inlet gas pressure (1, 2, 4, 6 MPa). The experimental results show: (a) the maximum permeability measured during the whole experiment is less than $10^{-17}$ m², which indicates that the gypsum interlayer has low permeability under high temperature and pressure that meet the requirements for radioactive waste repository. (b) Under the same temperature, the permeability of the gypsum specimen decreases at the beginning and then increases as the pore pressure elevates. When the inlet gas pressure is between 0 and 2 MPa, the Klinkenberg effect is very pronounced. Then, as the pore pressure increases, the movement behavior of gas molecules gradually changes from free motion to forced directional motion. So the role of free movement of gas molecules gradually reduced, which eventually leads to a decrease in permeability. When the inlet gas pressure is between 2 and 6 MPa, the Klinkenberg effect dribbles away, and the gas flow gradually obeys to the Darcy's law. Hence, the permeability increased with the increase in inlet gas pressure. (c) The curve of permeability versus temperature is divided into five stages based on its gradient. In the temperature range of 20–100 °C, the permeability of gypsum decreased slowly when the temperature decreased. From 100 to 200 °C, the permeability of gypsum increased dramatically when the temperature increased. However, a dramatic increase in permeability was observed from 200 to 450 °C. Subsequently, in the temperature range of 450–550 °C, due to closure of pores and fractures, the permeability of the specimens slowly lessened when the temperature increased. From 550 to 650 °C, the permeability of gypsum slightly increased when the temperature increased; (d) the micro-cracks and porosity obtained from the CT images show a high degree of consistency to the permeability evolution; (e) when compared to the permeability evolutions of sandstone, granite, and lignite, gypsum exhibits a stable evolution trend of permeability and has a much greater threshold temperature when its permeability increases sharply. The results of the paper may provide essential and valuable references for the design and

✉ Chen Jie
  chenjie_cqu@163.com

1  Mining Technology Institute, Taiyuan University of Technology, Taiyuan, Shanxi, China

2  College of Defense Engineering, PLA University of Science and Technology, Nanjing, Jiangsu, China

3  State Key Laboratory of Coal Mining Science and Dynamic Disaster Control, Chongqing University, Chongqing, China

construction of high-level radioactive wastes repository in bedded salt rock containing gypsum interlayers.

# 1 Introduction

While the development of the nuclear industry all around the world has brought great conveniences to humanity, the disposal of incidental nuclear waste has become a major problem. It is an optimal and acknowledged way to bury the high-level radioactive waste in a deep underground space after a great effort of study argumentations in it. Rock salt is one of the ideal candidate rocks because of its special properties, such as low permeability (Alkan 2009; Meng et al. 2015, 2016), compact microstructure (Liu et al. 2015, 2016), high heat conductivity, and self-healing capacity if damaged (Liang et al. 2006; Chen et al. 2013; Wang et al. 2015). In recent decades, rock salt formations have been widely utilized all around the world for the storage of hydrocarbons (natural gas, oil) (Li et al. 2014), the storage of compressed air (Zhang et al. 2015), and even the permanent disposal of nuclear wastes (Yang et al. 1999). Many countries have constructed a great number of underground caverns of oil, gas, and radioactive waste repositories in salt formations, especially the USA and Canada.

The mechanical properties and permeability of the surrounding rock are key parameters to evaluate the safety and tightness of oil/gas caverns or the radioactive waste repositories in rock salt during the periods of site selection and designing. Seepage inevitably occurs in the process of storage for improper assessment, sometimes causing severe accidents (Wang et al. 2015). For instance, liquefied petroleum gas leakage from porous soil occurred in the Barbers' Hill dome in 1980, Texas, and caused a severe explosion (Thoms and Gehle 2000; Evans 2009). A similar accident happened again at the same site five years later. In 1992, a serious explosion occurred in the Brenham salt dome in Texas because of liquefied petroleum gas leak from salt cavern. Fortunately, no reports on the leakage of radioactive wastes have been seen until now. Regardless of how and where a leakage of nuclear material takes place, it will always be a great hazard. Therefore, investigating the mechanical properties and permeability evolution of the surrounding rock reasonably and accurately is a key element in the safety of the operation and the avoidance of inestimable loss.

As for the mechanical properties and permeability of the surrounding rock, there are a great number of studies that have been carried out during the past decades. Ranjith et al. (2012) carried out Uniaxial Compressive Strength (UCS) testing of Hawkesbury sandstone at various temperatures between 25 and 950 °C. Gan and Elsworth (2016) and Indraratna et al. (1999) studied the effects of stress state, joint orientation, external stress, and fracture orientation on the evolution of fracture permeability and flow rate. Stormont and Daemen (1992) investigated the gas permeability and the porosity of rock salt under two stress paths: hydrostatic state compression and conventional triaxial state compression. In addition, Alkan (2009) proposed a new percolation model to predict the dilatancy-induced permeability increase in the excavation disturbed zone based on semi-empirical approaches considering the crack conductivity and network connectivity. However, gypsum interlayers (mainly $CaSO_4 \cdot 2H_2O$), as a type of sedimentary rock, intersect the bedded salt deposits in China. The research results above all show the permeability of rock salt, granite, sandstone under different conditions, but there are rare reports on the permeability of the gypsum interlayer. Therefore, the permeability and porosity of non-salt interlayer (gypsum) is an essential research subject for the safety and tightness of salt beds in China.

Unlike the storage facilities of oil and gas in salt caverns, high-level radioactive waste will emit a large amount of heat and hydrogen during the disposal of radioactive substances. This causes the temperature of the surrounding rock to rise sharply; the temperature can usually reach to the range of 200–1000 °C (Zuo et al. 2016). Further thermal physical and chemical reactions will occur in the surrounding rock due to high temperature, especially when the gypsum interlayers are within the salt cavern. In addition, gypsum will undertake a series of chemical reactions with the increase in temperature, which may change the microstructure of the gypsum and induce severe damage. The damage of the gypsum at high temperature and pressure has a significant influence on the permeability and porosity of the surrounding rock (Strydom et al. 1995; Strydoma and Potgieterb 1999) as the radioactive waste repository. Therefore, in order to accurately evaluate the sealing and safety performance of a radioactive waste disposal repository which contains gypsum interlayers, the permeability and porosity of the gypsum interlayer under high temperature and triaxial pressure should be investigated thoroughly.

In this paper, we implemented a series of experiments of gypsum interlayer under high temperature and triaxial pressure and then explored the permeability evolution of the gypsum interlayer with the increase in temperature. In addition, every specimen was scanned in a micro-CT scanner at each testing temperature, and the development of the micro-cracks and porosity of the specimen with the increase in temperature were observed. Combined with the

test data and MCT images, the mechanism of the permeability along with the variation of temperature and pore pressure was analyzed specifically. The conclusion of our research can provide reliable design parameters for the site selection and construction of radioactive waste repositories in bedded rock salt with gypsum interlayers in China, and offer theoretical guidance to relevant studies.

## 2 Experimental Apparatus and Procedure

### 2.1 Description of Experimental Rig and the Measurement Parameter

A self-designed solid-head coupled triaxial rock permeability testing system is applied in this experiment, which consists mainly of a triaxial loading system, a gas pressurized system, and a heating system. The schematic of the test instrument is shown in Fig. 1. The triaxial loading system is composed of an axial part and a lateral part, which can provide a maximum pressure of 100 MPa. In order to study the permeability evolution of the surrounding rock, the experiment was carried out under a hydrostatic pressure of 25 MPa (both the axial pressure and confining pressure are 25 MPa) to simulate an in situ stress state. In addition, there is a small air hole in the axial jack, which is used to supply the pore pressure. The maximum pore pressure from the gas pressurized system is 10 MPa. Note that gypsum will dissolve in water, producing some cracks inside the gypsum and eventually leading to inaccurate experimental results. Hence, nitrogen ($N_2$) is used as the inert gas because it is nonpolluting and chemically stable under high pressure and temperature. There is a certain danger caused by the high pressure of gas, and accordingly, the maximum inlet gas pressure in the test is only loaded to 6 MPa. During the experiment, in order to

prevent gas from escaping through the side direction, the inlet gas pressure should be at least 2 MPa lower than the confining pressure (Niu et al. 2014). Temperature is controlled by an electric stove wire encircling the specimen, and a heat insulation device is used in the peripheral of the heating system to avoid heat loss. In the experiment, the specimens will be heated to 650 °C at most.

According to Darcy's law of steady-state gas method, the permeability can be calculated as follows (Jsainge et al. 2011):

$$\kappa = \frac{2\mu P_0 Q_0 L}{(P_1^2 - P_2^2)A} \tag{1}$$

where $\kappa$ is the gas permeability ($m^2$); $\mu$ is the dynamic viscosity of gas (MPa s); $P_0$ is the atmospheric pressure (0.1 MPa); $Q_0$ is the gas flow rate ($m^3 \ s^{-1}$); $L$ and $A$ are the length and sectional area of the specimen (m, $m^2$); $P_1$ and $P_2$ are the inlet gas pressure and outlet gas pressure, respectively (MPa), usually $P_2 = P_0 = 0.1$ MPa. Accordingly, the gas flow rate, the inlet gas pressure, and the outlet pressure of $N_2$ will be measured in the process of testing to calculate the permeability. The length and sectional area of the specimens were measured before the test, and slight deformation of the specimen will be ignored during the experiment.

### 2.2 Preparation for Rock Specimen and Experimental Procedure

In this test, three specimens taken from one gypsum interlayer in Yunying area, Hubei Province, central China, located at a depth of 1200 m were cut to the given dimensions (diameter 50 mm, length 100 mm) to suit the triaxial compression chamber appropriately. The size of the three specimens is $\phi$ 49.9 × 99.4 mm, $\phi$ 49.9 × 99.8 mm and $\phi$ 49.9 × 100.2 mm, respectively.

The power from the gypsum interlayer was polished for the chemical composition determination by XRD (X-Ray determination). The spectral peaks of the various components are shown in Fig. 2, and the content of them is presented in Table 1.

The tests were carried out on the three specimens under a fixed hydrostatic pressure. The temperature was varied from room temperature to 650 °C, and the inlet gas pressure was varied from 1 to 6 MPa. The axial and confining pressures were gradually increased to 25 MPa after the specimen was installed. When the gas flow became stable in the specimen matrix, the permeability of the gypsum specimen was tested at the initial temperature (at room temperature of 20 °C) with the inlet gas pressures of 1, 2, 4, and 6 MPa, respectively. The inlet gas pressure should be maintained for at least 15 min so as to gather an adequate amount of gas and measure a stable flow rate
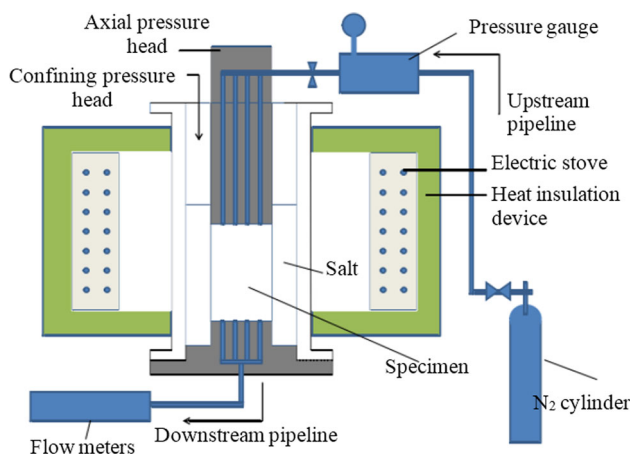


**Fig. 1** Illustration of the self-designed solid-head coupled triaxial rock permeability testing system
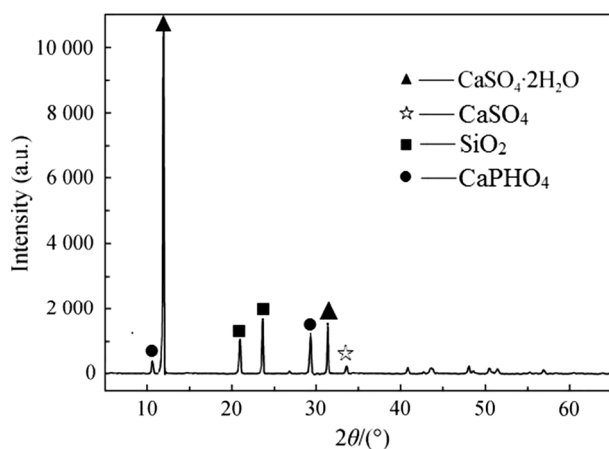
**Fig. 2** XRD scan of gypsum interlayer

under a corresponding inlet gas pressure. In addition, the measurements of relevant parameters at each pore pressure should be repeated at least three times to guarantee the precision of the results. When the first test of the permeability was accomplished under all the inlet gas pressures, the specimen was heated at a rate of 10 °C/min to the next testing temperature. The specimen was hold for at least 4 h at every testing temperature in order to ensure that the specimen was entirely and uniformly heated to the required temperature, and also to ensure that the contingent

chemical and physical reactions occur adequately (Olgaard et al. 1995). The highest test temperature selected was 650 °C, and the permeability test was conducted every 50 °C under different pore pressures (1, 2, 4, 6 MPa) started at 20 °C (the room temperature). Three specimens were tested in sequence according to the above process. The data of the all tests were recorded and used to calculate the permeability of the gypsum, as shown in the following Table 2.
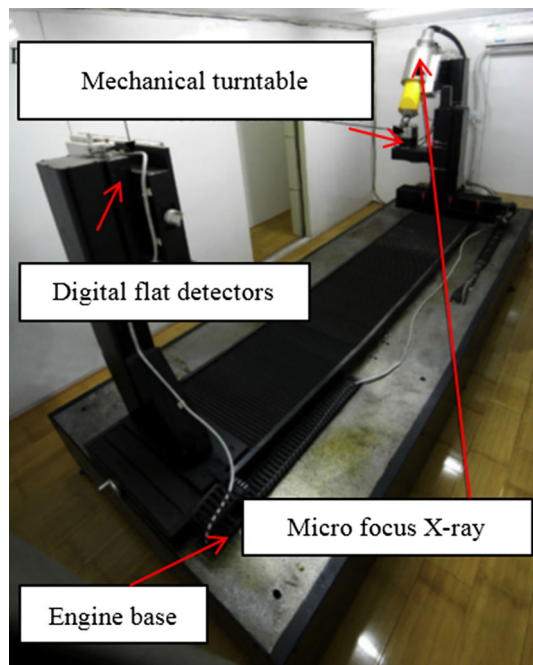
### 2.3 MCT test

The $\mu$-CT225kvFCB micro-CT experimental system (MCT) was designed by the Taiyuan University of Technology and Applied Electronics Institute, Academy of Engineering Physics of China, which consists of an X-ray machine, a digital flat-panel detector, and other assemblies, as shown in Fig. 3. The minimum scanning unit size of the MCT experimental system is 0.5 μm, which indicates that the system is capable of discriminating a micro-crack and pore of less than 1 μm width. When all the permeability measurements are accomplished at each testing temperature, the specimen will be moved from the triaxial compression chamber to the MCT system and scanned. MCT images are obtained after scanning the specimens. The dark areas in the MCT images present regions of low density,

**Table 1** Compositions and contents of the tested specimens (mean value)

| Chemical component | Gypsum ($CaSO_4 \cdot 2H_2O$) | Quartz | Brushite | Anhydrite | Sophiite |
|---|---|---|---|---|---|
| Content (%) | 85.4 | 8.7 | 4.8 | 0.7 | 0.4 |

**Table 2** Permeability with respected with different temperature and inlet gas pressure ($\times 10^{-17}$ m$^2$)

| Temperature (°C) | Inlet gas pressure (MPa) | | | | | | | | | | | |
|---|---|---|---|---|---|---|---|---|---|---|---|---|
| | #1 | | | | #2 | | | | #3 | | | |
| | 1 | 2 | 4 | 6 | 1 | 2 | 4 | 6 | 1 | 2 | 4 | 6 |
| 20 | 0.106 | 0.099 | 0.114 | 0.115 | 0.084 | 0.081 | 0.089 | 0.096 | 0.056 | 0.062 | 0.069 | 0.074 |
| 50 | 0.109 | 0.092 | 0.106 | 0.112 | 0.078 | 0.069 | 0.083 | 0.091 | 0.054 | 0.053 | 0.064 | 0.069 |
| 100 | 0.116 | 0.083 | 0.094 | 0.117 | 0.052 | 0.053 | 0.055 | 0.059 | 0.051 | 0.046 | 0.055 | 0.062 |
| 150 | 0.274 | 0.241 | 0.351 | 0.323 | 0.085 | 0.080 | 0.092 | 0.107 | 0.062 | 0.057 | 0.069 | 0.074 |
| 200 | 0.353 | 0.342 | 0.415 | 0.448 | 0.129 | 0.106 | 0.145 | 0.176 | 0.095 | 0.112 | 0.117 | 0.142 |
| 250 | 0.724 | 0.521 | 0.971 | 1.132 | 0.342 | 0.277 | 0.426 | 0.672 | 0.214 | 0.165 | 0.364 | 0.552 |
| 300 | 1.121 | 0.882 | 1.452 | 1.783 | 0.768 | 0.515 | 0.835 | 1.420 | 0.509 | 0.426 | 0.875 | 1.118 |
| 350 | 1.962 | 1.621 | 2.231 | 2.782 | 1.513 | 1.218 | 1.924 | 2.312 | 0.996 | 0.724 | 1.224 | 1.895 |
| 400 | 2.533 | 2.124 | 2.874 | 3.241 | 1.941 | 1.433 | 2.342 | 2.735 | 1.463 | 1.024 | 1.787 | 2.295 |
| 450 | 2.618 | 2.771 | 2.913 | 3.079 | 1.944 | 1.484 | 2.417 | 2.799 | 1.589 | 1.214 | 1.925 | 2.322 |
| 500 | 2.557 | 2.218 | 2.816 | 2.890 | 1.824 | 1.357 | 2.289 | 2.534 | 1.154 | 1.577 | 1.643 | 1.965 |
| 550 | 2.318 | 2.017 | 2.665 | 2.784 | 1.625 | 1.199 | 1.991 | 2.214 | 1.054 | 1.243 | 1.632 | 1.843 |
| 600 | 2.428 | 2.237 | 2.443 | 2.895 | 1.706 | 1.267 | 2.125 | 2.284 | 1.221 | 1.007 | 1.785 | 2.247 |
| 650 | 2.427 | 2.243 | 2.556 | 2.991 | 1.709 | 1.288 | 2.221 | 2.293 | 1.218 | 1.019 | 1.882 | 2.199 |

**Fig. 3** $\mu$-CT225kvFCB MCT test system of Taiyuan University of Technology



**Fig. 4** Permeability of the specimen versus pore pressure at different temperatures (°C)

whereas the bright areas represent high-density regions. By analyzing the MCT slides and pixels, we can clearly determine the morphological distribution of the rock particles and the distributions of pores and fissures. It is worth to note that the conventional thresholding techniques for quantifying the porosity of rock have been compared by many researchers who have found that these methods (for example, global thresholding), which are additionally hampered by the frequent presence of artifacts in MCT databases, usually fail to extract narrow cracks and low porosity. In this paper, we therefore chose to apply the 2D/3D voxel-based segmentation using the multi-scale Hessian filter (MSHFF) of Voorn et al. (2013). This approach, which is not computationally demanding, can precisely extract the fractures and apertures from the MCT database, and also a better estimation of the micro-porosity for rock types with smaller ranges of pore sizes. The MSHFF method has been implemented as a macro-code in the open-source software FIJI using the Feature J plugin.

## 3 Experimental Results and Discussion

In the present study, to minimize experimental error, there were three gypsum specimens selected in the experiment to investigate the permeability evolution versus the variation of temperature and gas pore pressure. The same variation trend of the three groups of the experimental data certifies the accuracy of the test process, although part of the data is

different. This is probably due to the difference of content and distribution of the component impurities (Such as, Quartz, Brushite, Anhydrite, Sophiite, as shown in Table 1). In order to simplify the analysis of the data, only one group of test data (#2) is selected and discussed in detail in the paper, as shown in Table 2. The instrument using the method of steady-state gas flow has a permeability measuring precision of up to $10^{-20}$ m$^2$. Hence, the data we get from the experiment are reliable.

### 3.1 Experimental Analysis of Pore Pressure Effect on Permeability of Gypsum

A general trend observed in Fig. 4 is that the permeability decreased as the temperature increased in the initial phases, but increased as the temperature increased in the latter phases. With the increase in the inlet gas pressure, the permeability decreased at first and then increased, showing a "V" shape tendency. The permeability curve can be divided into two stages separated by the lowest point. Here we would like to discuss these two stages specifically.

*Stage I* The permeability of gypsum decreased at first when the inlet gas pressure rose from 1 to 2 MPa under any temperature. This phenomenon was consistent with other experimental results, such as the permeability experiment of mudstone (Billiotte et al. 2008), rock salt (Cosenza et al. 1999), and coal (Zhu et al. 2007). The dramatic decrease in permeability along with the increase in pore pressure is mainly due to the Klinkenberg effect. The free molecular movement plays a decisive role at this stage. The movement behavior of gas molecules gradually changes from free motion to forced directional motion. So the role of free movement of gas molecules gradually reduced and eventually led to a decrease in permeability. Theoretically, the permeability needs to be modified by adopting the Klinkenberg equation; however, this paper focuses mainly

on the mechanism of the evolution of the permeability; thus, the correction on the permeability was not carried out.
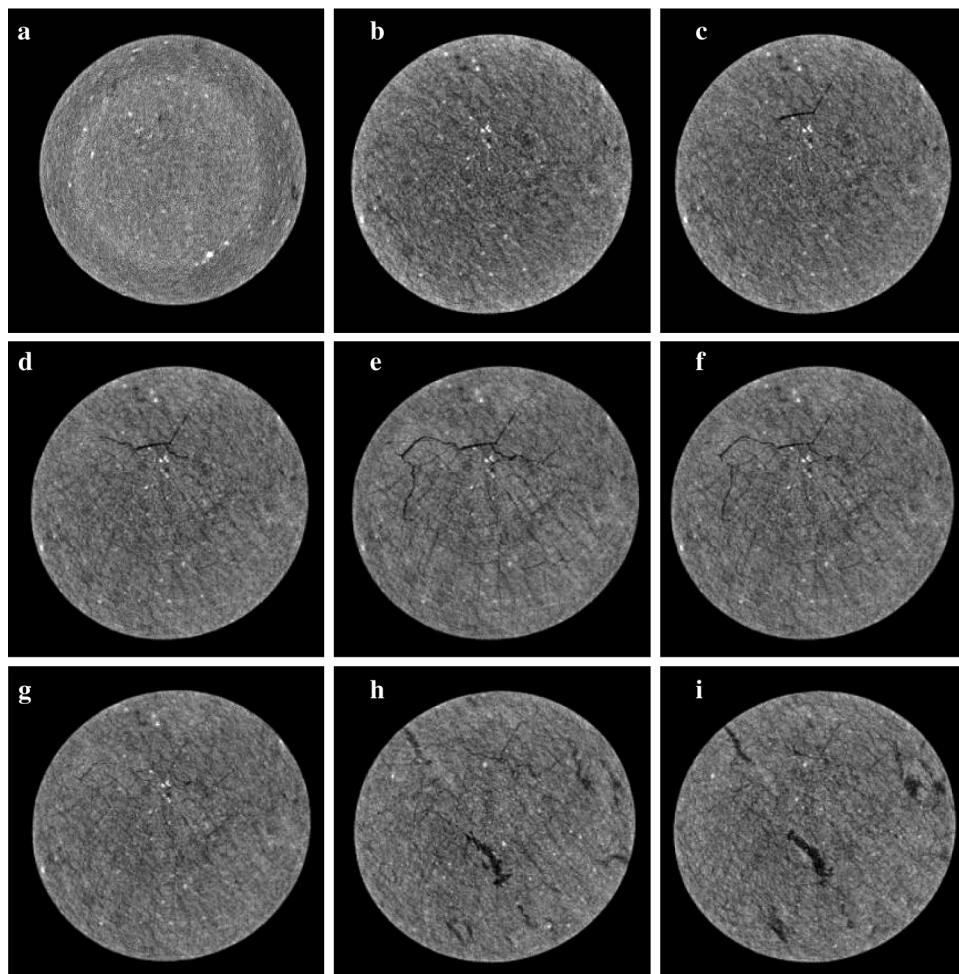
*Stage II* Apparent changing characteristics of the permeability can be observed when the inlet gas pore pressure ranges from 2 to 6 MPa. The permeability increased when
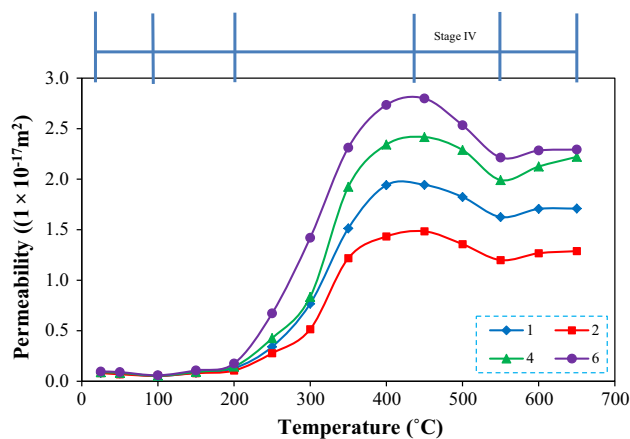


**Fig. 5** Permeability of the specimen versus temperature with different pressures

the inlet gas pressure increased. This is because, when the inlet gas pressure is between 2 and 6 MPa, the Klinkenberg effect dribbles away, and the gas flow gradually obeys to the Darcy's law. Besides, the most interesting thing is that the increasing rates of the permeability curve at respective temperatures is different, which will be delineated in details later.

## 3.2 Experimental Analysis of Temperature Effect on Permeability of Gypsum

The data presented in Table 2 are reproduced in a figure which shows the variation of gypsum permeability versus temperature, and the four curves can be obtained in Fig. 5. Obviously, the influence of temperature on the permeability of gypsum seems more complex. In addition, the tendency that the internal porosity and micro-cracks of the specimen developed with the temperature increase has a consistence with the variable trend of the permeability (see Figs. 6, 7), which indicates that the porosity and permeability of the specimen are positively related and have a similar agreement with the conclusion of Okazaki et al.

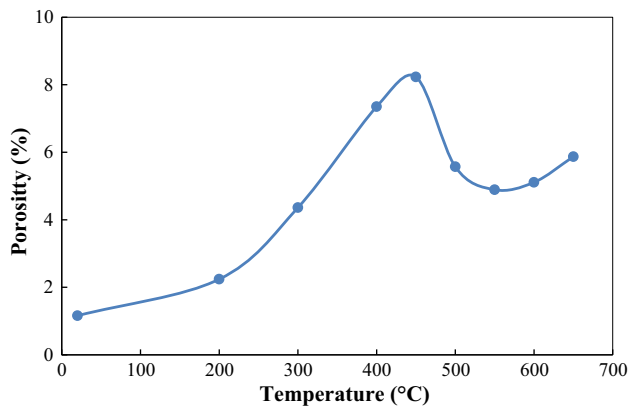**Fig. 6** X-ray MCT image example of same specimen under the different temperature. **a** Slice at 25 °C. **b** Slice at 200 °C. **c** Slice at 300 °C. **d** Slice at 400 °C. **e** Slice at 450 °C. **f** Slice at 500 °C. **g** Slice at 550 °C. **h** Slice at 600 °C. **i** Slice at 650 °C
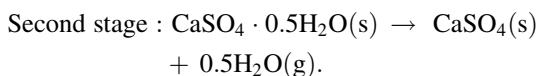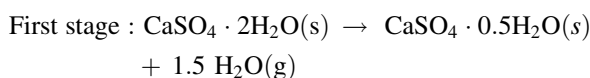
**Fig. 7** Porosity as a function of the temperature

(2014) and Zhu et al. (2007). In Fig. 5, the permeability curves under four values of inlet gas pressure exhibit the same variational trend. In order to simplify the analysis process, we chose one of the permeability curves in this section to discuss the temperature effect on the permeability in detail. As the temperature increases from 20 to 650 °C, the permeability curve can be divided into five stages based on their various gradients. Considering the high pore pressure during the disposal in the salt beds, here we particularly chose the permeability curve at the inlet gas pressure of 6 MPa as an example and discuss these five stages specifically combined with the MCT images as follows:

*Stage I* As seen in Stage I in Fig. 5, a slight decrease in the permeability can be observed with the rise of temperature from 20 to 100 °C under the inlet gas pressure of 6 MPa. There is no chemical reaction for contribute to the stability property of gypsum in this temperature range. However, the thermal expansion effect of the specimens becomes more obvious with the increase in temperature. The expansion deformation of the gypsum specimen has been constrained by the high axial and confining pressures, which results in the closure of internal voids and microcracks and causes the decrease in the permeability.

*Stage II* The permeability of the gypsum specimen begins to increase slowly from 100 to 200 °C. According to the analysis of chemical compositions on the gypsum before the experiment, the main part of the specimens is $CaSO_4 \cdot 2H_2O$ (approximately 85.4%). Strydom et al. (1995) and Olgaard et al. (1995) presented that the dehydration of $CaSO_4 \cdot 2H_2O$ will occur in this temperature zone in the following two stages:

$$First\ stage : CaSO_4 \cdot 2H_2O(s) \rightarrow CaSO_4 \cdot 0.5H_2O(s) + 1.5\ H_2O(g)$$

$$Second\ stage : CaSO_4 \cdot 0.5H_2O(s) \rightarrow CaSO_4(s) + 0.5H_2O(g).$$

In the first stage, the dehydration reaction of gypsum mainly takes place in the temperature range of 95–170 °C and will lose most of the crystal water. The second stage occurs in the process of the first stage, when the temperature exceeds 172 °C. No hemihydrate could be observed for a complete reaction (Strydom et al. 1995). Accordingly, due to the thermal dehydration and pyrolysis of gypsum interlayer, a range of crack types with a broad distribution of dimensions (length and width), orientations, and shapes appear on the gypsum crystal surface, which will result in a high porosity and permeability. As shown in Fig. 6a, b, it is noticeable to see the micro-cracks growth by comparing the MCT images at this stage. Also, many micro-cracks can be seen in the MCT images (not obvious), which represents that the tiny movement passageways formed among the pores during this temperature range. In addition, this phenomenon was consistent with the experimental conclusions of Sipple et al. (2001). However, it is time-consuming to be spent on forming more interconnected pores under the combined effects of temperature and pressure. The permeability increased slowly compared to the next stage, and the permeability increasing effect lags behind the growth of pore void ratio.

*Stage III* At this stage, the permeability of the gypsum specimen increases sharply with the increase in temperature. There is a comprehensive effect that results in the dramatic shift. First of all, all of the hydrous calcium sulfate loses the last part of water and this enhances its porosity (Strydom et al. 1995). However, the effect of the dehydration does not play a significant role in changing the permeability because it is difficult to lose the rest of the crystalliferous water in a short time. Then, thermal cracking will occur in the specimen during this temperature region. The propagation of the micro-cracks with the increase in temperature is the main reason for the sharp increase in permeability. From Fig. 6c–e, it is obvious to see the generation and expansion of micro-cracks, which is consistent with the increase in permeability. Thirdly, the damage of the porous medium is serious and easy to form connection holes, and thus redound to improving the permeability under the high hydrostatic pressure. At last, when the temperature rises to 350 °C, one can observe large-sized cracks appear. Then, with the increase in temperature, the density of the cracks gradually adds and reaches a maximum at 450 °C. However, in this temperature range, the permeability growth rate gradually decreases with increase in temperature. It can be explained through the variation rule that a high confining pressure starts to play a role in constraining the large deformation caused by the thermal cracking. Hence, the growth rate of the permeability begins to decrease.

*Stage IV* As observed in Fig. 5, the permeability in this temperature range appears slightly lower. This is because the gypsum grains became soft in this temperature range. Then, under the action of triaxial stress, the gypsum specimens underwent a large deformation, resulting in the closure of the pores and fractures. As the pores and fractures were closed, the penetration of nitrogen was obstructed, resulting in a lower permeability. The thermal cracking damage gets more and more server as the temperature increases, so that the specimen cannot bear high hydrostatic pressure for the serious internal deterioration and induces a large plastic deformation which declines the porosity and permeability. By comparing Fig. 6e with 6g, it is easy to find that a few cracks have been closed, which indicates that there is a large plastic deformation inside the specimen. Obviously, the thermal damage effect is covered by the effect of the plastic deformation, which makes the permeability decrease. However, the anhydrous gypsum produced by the gypsum dehydration is harder and has a higher thermal stability. The anhydrous and the impurities (mainly quartz) in the natural gypsum can also form a skeleton in the specimen and limit the plastic deformation of the specimen. Based on the above reasons, the decrease in permeability of the specimens is not very dramatic.

*Stage V* In this stage, the permeability has a slight increase after 550 °C. Thermal cracking continues to generate new cracks as the temperature increases, which causes the permeability to increase slightly. The new damage can be seen in the corresponding MCT images.

The cracks induced by thermal cracking will increase the value of the porosity. The more cracks that are generated as the temperature rises, the higher the permeability will be. The initial porosity we tested of the gypsum specimen is about 1–1.2%. After thermal cracking, the porosity will increase because new cracks occupy the space of the voids. The results are listed in Fig. 7. As seen in this picture, the variation of the porosity versus temperature has similar trends with that of the permeability versus temperature. This further certified our interpretation of the permeability evolution of the gypsum under high temperatures.

In order to clarify the chemical mechanisms of gypsum under different temperature ranges, the pyrolysis behavior of the gypsum interlayer was investigated at a heating rate of 20 °C/min in a thermogravimetric analyzer (Mettler Toledo TGA/SDTA851e). During the experiment, about 50 mg of the gypsum interlayer was placed in an 80 mL ceramic crucible and pyrolyzed under a 30 mL/min $N_2$ flow from 25 to 650 °C. The composition of the gas product was analyzed using gas chromatography, Model 7890II, with a thermal conductive detector.

The thermogravimetric (TG) and the differential thermogravimetric (DTG) curves of the gypsum interlayer at different heating rates are shown in Fig. 8. From the figure, it can be seen that the mass loss observed between 80 and 200 °C is due to the loss of the hydrated water of calcium sulfate. The dissociation of the chemical bound water takes place in two stages. In the first stage, the calcium sulfate dihydrate loses 75% of its water, thus forming calcium sulfate hemihydrate ($CaSO_4 \cdot 5H_2O$). If the gypsum is further heated, a second reaction occurs, where the calcium sulfate hemihydrate loses the remaining water to form calcium sulfate anhydrate ($CaSO_4$). Accordingly, due to the thermal dehydration and pyrolysis of the gypsum interlayer, a range of crack types with a broad distribution of dimensions (length and width), orientations, and shapes appear on the gypsum crystal surface (Sipple et al. 2001). This results in a high porosity and permeability. In the temperature range of 450–550 °C, the permeability of the specimens slowly decreased when the temperature increased. This is because the gypsum grain became soft in this temperature range. Then, under triaxial stress, the gypsum specimens underwent a large deformation, resulting in the closure of the pores and fractures. As the pores and fractures were closed, the penetration of the nitrogen was obstructed, resulting in a lower permeability. In order
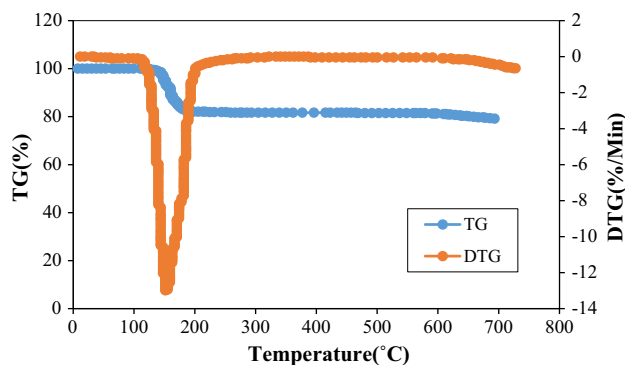


**Fig. 8** TG and DTG curves
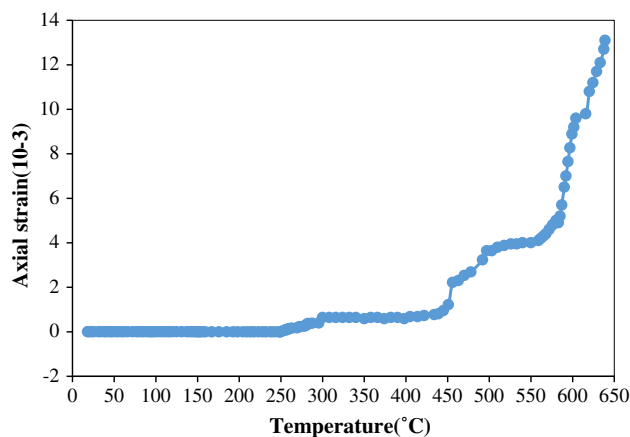


**Fig. 9** Relationship between axial strain and temperature

to clarify the physical mechanism, the relationship between axial strain and temperature is illustrated in Fig. 9. Obviously, in the temperature range of 20–450 °C, the strain is small and increases slowly. However, in the temperature range of 450–650 °C, the axial strain increases rapidly and varies from 1.22 to 13.1%. Most likely, the gypsum specimens became more compact, which leads to a decrease in permeability. This can strongly support the decrease in the permeability of gypsum in this temperature range. Also, the variational trend of fractures in the MCT images can explain the phenomenon (i.e., the decrease in permeability) well.

### 3.3 Experimental Investigation of the Combined Effect of Temperature and Pressure on Permeability of Gypsum

The separate effects of temperature and pore pressure on the permeability of gypsum have been discussed in Sects. 3.1 and 3.2, while the combined effects of the temperature and pressure on the permeability of gypsum will be analyzed in detail in this section. In order to explain the combined effects clearly, further information is presented in the following parts based on Figs. 4 and 5.

As shown in Fig. 4, in the range of 1–2 MPa, the permeability decreased with the increase in pore pressure due to Klinkenberg effect. It is interesting to note that, in the temperature range of 20–400 °C, the difference of permeability (i.e., the difference between the permeability under 1 MPa and its permeability under 2 MPa) gradually increases with the increase in temperature; whereas when the temperature exceeds 400 °C, the difference value of permeability stays stable. This phenomenon may be caused by two reasons.

According to the Knudsen number (Firouzi et al. 2004)

$$K_n = \frac{\lambda}{r} \tag{2}$$

where in $\lambda$ and $r$ represent the mean free path of the gas molecules and the average pore radius, respectively. And the mean free path is given by

$$\lambda = \frac{k_B T}{\pi d^2 p \sqrt{2}} \tag{3}$$

where $k_B$ is the Boltzmann constant, $T$ is the absolute temperature, $d$ is the gas molecular diameter, and $P$ is the gas pressure.

On the one hand, when the temperature and pore pressure are relatively low, the gas can expand, and the mean free path of the gas molecules is proportional to the temperature and pore pressure. On the other hand, due to thermal expansion, the average pore radius will decline. In view of these, the Knudsen number is very large, and

slippage effect is also significant. When the temperature is more than 100 °C, a series of chemical reactions and substrate degradations take place, resulting in the complex variable trend of the slippage effect with the temperature growth. For example, in Stage II in Fig. 4, when the temperature is below 300 °C, permeability increased significantly with the increase in pore pressure. However, when the temperature exceeded 350 °C, the high temperature and pressure resulted in the matrix softening and a large plastic deformation of the specimen, which closed the pores and fractures in the test time. That is why the permeability increases slowly when the pore pressure increases, and the permeability almost has no change under 650 °C when the inlet gas pressure increases from 4 to 6 MPa.

From Fig. 5, one can interpret another phenomenon that is caused by the combined effect of temperature and pressure. When the temperature is below 100 °C, the permeability of the gypsum specimen is almost constant under varying pore pressures. In addition, when the temperature exceeds 550 °C, the permeability of the specimen under two pore pressures of 4 and 6 MPa is close to each other. This is mainly caused by the plastic deformation because of the persistent effect of the triaxial confining pressure.

## 4 The Comparison of Permeability Between Sandstone, Granite, Lignite and Gypsum

Based on the fact that the permeability of rock at elevated temperatures plays an important role in the technical aspects of engineering field, our study team carried out a series of permeability experiments on assorted rocks under high temperatures. Zhao et al. (2017) conducted an experiment on the permeability evolution of sandstone and granite under high temperature and pressure by using a 20 MN servo-controlled rock triaxial testing machine with high temperature and high pressure. In addition, Niu et al. (2014) investigated the permeability of lignite under elevated temperature and pressure based on the same experimental facility used in this paper. In order to investigate the essential differences in the permeability properties of rocks, we have collected those curves of permeability versus temperature of the several types of rock and drawn them in the same picture for comparing, as shown in Fig. 10.

The permeability curves of sandstone, granite, Lignite, and gypsum with temperature increases are illustrated in Fig. 10. Considering the different test conditions, here we only discuss the variational trends of the rocks' permeability versus temperature rather than the magnitude of the permeability. An obvious sudden change appears in the permeability curves for the sandstone and granite, while that of the lignite and gypsum are relatively flat. The main reason is that the different thermal expansion coefficients of the various components produce hot
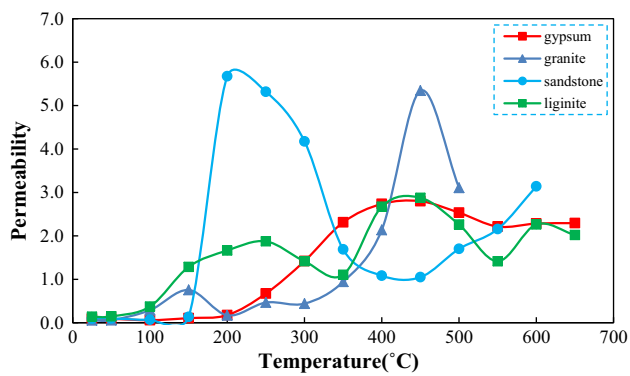
**Fig. 10** Permeability of sandstone ($1 \times 10^{-17}$ m$^2$), granite ($1 \times 10^{-18}$ m$^2$), lignite ($1 \times 10^{-14}$ m$^2$) and gypsum ($1 \times 10^{-17}$ m$^2$) (Zhao et al 2017; Niu et al 2014)

cracking with temperature growth, and the specimens show brittle cracking. Comparatively, pyrolysis reactions occur in the specimen of lignite at high temperatures and induce the specimen to crack persistently with the increase in temperature. The fluctuation of the permeability curves comes from the comprehensive effect of the confining pressure and the temperature. However, the permeability rule of the temperature of gypsum is different from the above rock. However, when the temperature is low (lower than 100 °C), the two rock permeability laws are similar. In the range of 100–200 °C, the gypsum loses a lot of its crystallization water, inducing the specimen to generate a large amount of pores which may cause severe internal damage. As the temperature continues to rise, the specimen begins to produce thermal cracks which induce the permeability to rise at a relatively rapid rate. In addition, granite is another type of rock to be used as a host rock for radioactive waste disposal. However, the threshold temperature of when the permeability increases sharply of granite is approximately 200 °C, which is almost same as that of gypsum (approximately 200 °C). Besides, the absolute increment of permeability of gypsum is also much less than that of granite. Therefore, gypsum seems appropriate as the host rock for radioactive waste disposal.

When the temperature is over 450 °C, the small variation in the permeability of gypsum is mainly due to the interaction between the thermal fractures and the specimen deformation. Limited to the test conditions, the maximum temperature in this experiment is 650 °C, and thus the permeability of gypsum when the temperature exceeds 800 °C remains to be further explored for the initiation of gypsum self-decomposition.

## 5 Conclusion

This paper reports the permeability of gypsum under different inlet gas pressures (1, 2, 4, 6 MPa) and temperatures (25–650 °C) by using the steady-state gas (nitrogen)

method on the triaxial rock permeability testing system. In addition, the MCT tests were conducted using the $\mu$-CT225kvFCB MCT test system to indicate the micromechanism of the permeability experiment. Combined with the discussion above, some conclusions are obtained as following:

(1) The maximum permeability of the gypsum recorded in the experiment is $2.991 \times 10^{-17}$ m$^2$, which shows the gypsum is still a low permeability medium under high temperatures (less than 650 °C) and hydrostatic pressure (25 MPa).

(2) When the inlet gas pressure is between 0 and 2 MPa, the Klinkenberg effect is very pronounced. Then, as the pore pressure increases, the movement behavior of gas molecules gradually changes from free motion to forced directional motion. So the role of free movement of gas molecules gradually reduced, which eventually led to a decrease in permeability. When the inlet gas pressure is between 2 and 6 MPa, the Klinkenberg effect dribbles away, and the gas flow gradually follow Darcy's law. The permeability increased with the increase in inlet gas pressure.

(3) The porosity of gypsum shows complex change trends with the increase in temperature according to the MCT images, and its variation trend is consistent with that of the permeability. Under the fixed pore pressure, the curve of permeability versus temperature is divided into five stages according to the variational trends. In the temperature range of 20–100 °C, the permeability of gypsum decreased slowly when the temperature decreased. From 100–200 °C, the permeability of gypsum increased dramatically when the temperature increased. However, a dramatic increase in permeability was observed from 200 to 450 °C. Subsequently, in the temperature range of 450–550 °C, due to the closure of pores and fractures, the permeability of the specimens slowly decreased when the temperature increased. From 550–650 °C, the permeability of gypsum slowly increased when the temperature increased.

(4) Gypsum exhibits a unique evolution characteristic and has its own mechanism of change with the increase in temperature in contrast to those of sandstone, granite, and lignite.

The valuable and desirable experimental data and law have been obtained for the permeability property of gypsum at high temperature and triaxial pressure, and our results can provide essential and valuable information for the design and construction of high-level radioactive waste repository in salt beds with gypsum interlayers in China.

# References

Alkan H (2009) Percolation model for dilatancy-induced permeability of the excavation damaged zone in rock salt. Int J Rock Mech Min Sci 46:716–724

Billiotte J, Yang D, Su K (2008) Experimental study on gas permeability of mudstones. Phy Chem Earth 33(S1):S231–S236

Chen J, Ren S, Yang CH, Jiang DY, Li L (2013) Self-healing characteristics of damaged rock salt under different healing conditions. Materials 6:3438–3450

Cosenza P, Ghoreychi M, Bazargan-Sabet B, Marsily GD (1999) In situ rock salt permeability measurement for long term safety assessment of storage. Int J Rock Mech Min 36(4):509–526

Evans DJ (2009) A Review of underground fuel storage events and putting risk into perspective with other areas of the energy supply chain. Geol Soc Spec Publ Lond 313(1):173–216

Firouzi M, Alnoaimi K, Kovscek A, Wilcox J (2004) Klinkenberg effect on predicting and measuring helium permeability in gas shales. Int J Coal Geol 123(2):62–68

Gan Q, Elsworth DA (2016) continuum model for coupled stress and fluid flow in discrete fracture networks. Geomech Geophys Geo-Energy Geo-Resour 2(1):43–61

Garing C, Gouze P, Kassab M, Riva M, Guadagnini A (2015) Anti-correlated porosity–permeability changes during the dissolution of carbonate rocks: experimental evidences evidences and modeling. Transp Porous Med 107(2):595–621

Hao TS, Liang WG (2016) A new improved failure criterion for salt rock based on energy method. Rock Mech Rock Eng 49(5):1721–1731

Indraratna B, Ranjith PG, Gale W (1999) Single phase water flow through rock fractures. Geotech Geol Eng 17(3–4):211–240

Jsainge D, Ranjith PG, Choi SK (2011) Effects of effective stress changes on permeability of Latrobe Valleybrown coal. Fuel 90(3):1292–1300

Li YP, Liu W, Yang CH, Daemen JJK (2014) Experimental investigation of mechanical behavior of bedded rock salt containing inclined interlayer. Int J Rock Mech Min Sci 69(3):39–49

Liang WG, Xu SG, Zhao YS (2006) Experimental study of temperature effects on physical and mechanical characteristics of salt rock. Rock Mech Rock Eng 39(5):469–482

Liu W, Li YP, Yang CH, Daemen JJK, Yang Y, Zhang GM (2015) Permeability characteristics of mudstone cap rock and interlayers in bedded salt formations and tightness assessment for underground gas storage caverns. Eng Geol 193:212–223

Liu W, Chen J, Jiang DY, Shi XL, Li YP, Daemen JJK (2016) Tightness and suitability evaluation of abandoned salt caverns served as hydrocarbon energies storage under adverse geological conditions (AGC). Appl Energy 178:703–720

Meng T, Hu Y, Fang R (2015) Study of fracture toughness and weakening mechanisms in gypsum interlayers in corrosive environments. J Natur Gas Sci Eng 26:356–366

Meng T, Hu Y, Fang R (2016) Weakening mechanisms of gypsum interlayers from Yunying salt cavern subjected to a coupled thermo-hydro-chemical environment. J Nat Gas Sci Eng 30:77–89

Niu S, Zhao Y, Hu Y (2014) Experimental investigation of the temperature and pore pressure effect on permeability of lignite under the in situ condition. Transp Porous Med 101(1):137–148

Okazaki K, Noda H, Uehara S, Shimamoto T (2014) Permeability, porosity and pore geometry evolution during compaction of Neogene sedimentary rocks. J Struct Geol 62:1–12

Olgaard DL, Sc Ko, Wong TF (1995) Deformation and pore pressure in dehydrating gypsum under transiently drained conditions. Tectonophysics 245(3):237–248

Ranjith PG, Viete DR, Chen BJ (2012) Transformation plasticity and the effect of temperature on the mechanical behaviour of Hawkesbury sandstone at atmospheric pressure. Eng Geol 151:120–127

Sipple E-M, Bracconi P, Dufour P, Mutin J-C (2001) Microstructural modifications resulting from the dehydration of gypsum. Solid State Ion 141(1):447–454

Stormont JC, Daemen JJK (1992) Laboratory study of gas permeability changes in rock salt during deformation. Int J Rock Mech Min Sci Geomech Abstr 29:325–342

Strydom CA, Hudson-Lamb DL, Potgieter JH, Dagg E (1995) The thermal dehydration of synthetic gypsum. Thermochim Acta 269–270(1):631–638

Strydoma CA, Potgieterb JH (1999) Dehydration behaviour of a natural gypsum and a phosphogypsum during milling. Thermochim Acta 332(1):89–96

Thoms RL, Gehle RM (2000) A brief history of salt cavern use (keynote paper). In: Geertman RM (ed) Proceedings of 8th world salt symposium, vol I. Elsevier, pp 207–214

Voorn M, Exner U, Rath A (2013) Multiscale hessian fracture filtering for the enhancement and segmentation of narrow fractures in 3D image data. Comput Geosci 57:44–53

Wang T, Yan X, Yang H (2013) A new shape design method of salt cavern used as underground gas storage. Appl Energy 104(2):50–61

Wang TT, Ma HL, Yang CH, Shi XL, Daemen JJK (2015) Gas seepage around bedded salt cavern gas storage. J Nat Gas Sci Eng 26:61–71

Yang CH, Daemen JJK, Yin JH (1999) Experimental investigation of creep behavior of salt rock. Int J Rock Mech Min Sci 36(2):233–242

Zhang G, Li Y, Daemen JJK (2015) Geotechnical feasibility analysis of compressed air energy storage (CAES) in bedded salt formations: a case study in Huai'an city, China. Rock Mech Rock Eng 48(5):2111–2127

Zhao Y, Yang D, Liu Z, Feng Z, Liang W (2014) Problems of evolving porous media and dissolved glauberite micro-scopic analysis by micro-computed tomography: evolving porous media (1). Transp Porous Med 107(2):36–385

Zhao YS, Wan ZJ, Zhang Y, Feng ZJ (2017) Evolution of mechanical properties of granite at high temperature and high pressure. Geomech Geophys Geo-Energy Geo-Resour 108(2):1–12

Zhu WC, Liu J, Sheng JC, Elsworth D (2007) Analysis of coupled gas flow and deformation process with desorption and Klinkenberg effects in coal seams. Int J Rock Mech Min 44(7):971–980

Zuo JP, Wang XS, Mao DQ (2016) T-M coupled effects on cracking behaviors and reliability analysis of double-notched crustal rocks. Eng Fract Mech 158:106–115